M&C 2017 - International Conference on Mathematics & Computational Methods Applied to Nuclear Science & Engineering, Jeju, Korea, April 16-20, 2017, on USB (2017)

Iterative Properties of Parallel Block Jacobi-Integral Transport Matrix Method with Source Iteration Preconditioning

Dylan S. Hoagland* and Yousry Y. Azmy*

**Department of Nuclear Engineering, North Carolina State University, Raleigh, NC*
dshoagla@ncsu.edu, yyazmy@ncsu.edu

Abstract - *Parallel Block Jacobi - Integral Transport Matrix Method (PBJ-ITMM) is a previously developed transport iterative solution method which allows for solution of S_N equations on massively parallel computer systems without the use of complex sweep algorithms. Theory and experiments have shown PBJ-ITMM to suffer severe iterative slowdown in problems with optically thin cells. We conjecture that this slowdown occurs due to the asynchronous spatial domain decomposition which PBJ-ITMM employs becoming increasingly ineffective as optically thin cells make the converged solutions in distant cells more coupled to each other. We use the Source Iteration (SI) iterative method to precondition PBJ-ITMM both to assess the viability of the combined method (which we term PBJ-ITMM-SI) for mitigating this iterative slowdown as well as to study the iterative properties of PBJ-ITMM to help aid in future development of acceleration methods. We study the spectral radius of PBJ-ITMM-SI theoretically using a Fourier analysis as well as computationally to show that for a given scattering ratio, the spectral radius no longer approaches unity as the cells become optically thin. Our study enhances our general understanding of PBJ-ITMM's iterative process and establishes PBJ-ITMM-SI to be most effective in heterogeneous problems which contain both optically thin and optically thick cells.*

I. INTRODUCTION

PBJ-ITMM allows for a massively parallel transport solution to be obtained in unstructured grids without the use of complex sweep algorithms.[1] This is accomplished by dividing the spatial domain into multiple sub-domains, all of which are mathematically decoupled over a single iteration. With lagged incoming angular fluxes, full transport solutions are obtained over each sub-domain. The incoming angular fluxes are then updated using the outgoing angular fluxes from adjacent sub-domains and this iterative process repeats until convergence of the sub-domain interface fluxes is observed. While the benefit of a massively parallel solution in unstructured grids without highly complex sweep algorithms is alluring, it has been previously demonstrated through a Fourier analysis as well as computational experiments that *PBJ-ITMM*'s spectral radius approaches unity as the cell size tends towards zero, increasing the required number of iterations without bound.[2] We conjecture that the cause of *PBJ-ITMM*'s iterative slowdown in optically thin cells is due to the mathematical decoupling of distant sub-domains which become more physically coupled with optically thin cells due to the increased path length which particles travel.

We introduce *SI* preconditioning to study this slowdown and as a potential tool for reducing it. Before formulating the *PBJ-ITMM-SI* method, it is important to address the fact that parallel execution of *SI* in unstructured grids requires the complex sweep algorithms that *PBJ-ITMM* was introduced to avoid.[3],[4] For this reason, we assume that all mesh sweeps conducted for *SI* preconditioning are to be computed using standard serial sweeps. Therefore, we preface this study with the disclosure that improvement to *PBJ-ITMM*'s iterative properties due to *SI* preconditioning comes at the cost of only half of the iterative process being computed in a massively parallel system. Although this is an admittedly steep penalty, it comes with the potential of eliminating the approach of *PBJ-ITMM*'s spectral radius towards unity as cell size decreases, preventing the required number of iterations from becoming arbitrarily large.

In addition to studying the viability of *PBJ-ITMM-SI*, we analyze the results from this study in order to enhance our understanding of the underlying causes of *PBJ-ITMM*'s iterative slowdown. Eventually, an acceleration method for *PBJ-ITMM* which does not inhibit it's parallel nature as much would be desirable. But due to the *PBJ-ITMM*'s input requiring angular fluxes current acceleration methods which are used for accelerating *SI* cannot be used, as they only update scalar fluxes. We provide the observed evidence of *PBJ-ITMM*'s iterative behavior in order to aid in the future development of acceleration methods for *PBJ-ITMM*.

To analyze the iterative performance of *PBJ-ITMM-SI* we observe the spectral radius trends. We do this theoretically using a Fourier analysis which we then verify computationally. We then provide additional computational experiments to assess the effectiveness of *SI* preconditioning, including studies in heterogeneous problems.

II. THEORY

1. FORMALISM OF ITERATIVE SCHEMES

For this study, we consider the case of one cell per subdomain as this maximizes the amount of lagged information, and hence, represents the worst case scenario from an iterative robustness standpoint. Additionally, we consider the *AHOT-N0* method for obtaining the needed auxiliary equations. For a 2-D problem with these specifications, the corresponding transport equation for a non-multiplying medium with an isotropic external source becomes the following, written for PBJ-ITMM iteration *(s+1/2)*. [5] Note that these equations must also be supplemented by boundary conditions.

$$\nu_{x,m,k,j}\left(\psi^{x+,(s+\frac{1}{2})}_{m,k,j} - \psi^{x-,(s)}_{m,k,j}\right) + \nu_{y,m,k,j}\left(\psi^{y+,(s+\frac{1}{2})}_{m,k,j} - \psi^{y-,(s)}_{m,k,j}\right) + \psi^{(s+\frac{1}{2})}_{m,k,j} = \frac{c_{k,j}}{4\pi}\phi^{(s+\frac{1}{2})}_{k,j} + \frac{1}{4\pi\Sigma_{t,k,j}}q_{k,j} \quad (1a)$$

$$\psi^{(s+\frac{1}{2})}_{m,k,j} = \frac{1+\alpha_{u,m,k,j}}{2}\psi^{u+,(s+\frac{1}{2})}_{m,k,j} + \frac{1-\alpha_{u,m,k,j}}{2}\psi^{u-,(s)}_{m,k,j} \quad (1b)$$

$$\phi^{(s+\frac{1}{2})}_{k,j} = \sum_{m=1}^{M} w_m \psi^{(s+\frac{1}{2})}_{m,k,j} \quad (1c)$$

where,

$$\nu_{x,m,k,j} \equiv \frac{|\Omega_{u,m}|}{\Sigma_{t,k,j}\Delta u_{k,j}} \quad (2)$$

The subscript m denotes the discrete ordinate index and subscripts k and j correspond to cell (k, j). Additionally, w_m corresponds to the quadrature's m^{th} angular weight, c is the scattering ratio, and the $u+$ and $u-$ superscript on the angular flux variables denote evaluation on outgoing and incoming edges, respectively, on the edges of cell (k,j), $u = x$ or y. These equations are valid for any *Weighted Diamond Difference* (*WDD*) scheme. In particular, we are interested in the *AHOT-N0* method, for which we use the following equation.[6]

$$\alpha_{u,m,k,j} = \coth\left(\frac{\Sigma_{t,k,j}\Delta u_{k,j}}{2|\Omega_{u,m}|}\right) - \frac{2|\Omega_{u,m}|}{\Sigma_{t,k,j}\Delta u_{k,j}} \quad (3)$$

Note that in Eqs. (1), the only quantities that are lagged to iteration s are the incoming angular fluxes. Hence, this represents a full transport solution over each sub-domain, assuming a prescribed incoming boundary angular flux.

To implement *SI* preconditioning, we then introduce the following equations which, like Eqs. 1, must also be supplemented by boundary conditions.

$$\nu_{x,m,k,j}\left(\psi^{x+,(s+1)}_{m,k,j} - \psi^{x-,(s+1)}_{m,k,j}\right) + \nu_{y,m,k,j}\left(\psi^{y+,(s+1)}_{m,k,j} - \psi^{y-,(s+1)}_{m,k,j}\right) + \psi^{(s+1)}_{m,k,j} = \frac{c_{k,j}}{4\pi}\phi^{(s+\frac{1}{2})}_{k,j} + \frac{1}{4\pi\Sigma_{t,k,j}}q_{k,j} \quad (4a)$$

$$\psi^{(s+1)}_{m,k,j} = \frac{1+\alpha_{u,m,k,j}}{2}\psi^{u+,(s+1)}_{m,k,j} + \frac{1-\alpha_{u,m,k,j}}{2}\psi^{u-,(s+1)}_{m,k,j} \quad (4b)$$

$$\phi^{(s+1)}_{k,j} = \sum_{m=1}^{M} w_m \psi^{(s+1)}_{m,k,j} \quad (4c)$$

To implement the *PBJ-ITMM-SI* iterative method, Eqs. (1) are solved for each sub-domain simultaneously by constructing and solving the matrix associated with the local system of equations. The result from this solution which is then passed to the *SI* iterative scheme in Eqs. (4) is the cell averaged scalar flux, $\phi^{(s+\frac{1}{2})}_{k,j}$. Equations (4) are then solved globally using a single mesh sweep per direction. From the *SI* solution, the cell outgoing angular fluxes, $\psi^{x+(s+1)}_{m,k,j}$ and $\psi^{y+(s+1)}_{m,k,j}$ are passed to the next iteration as the incoming angular fluxes to adjacent sub-domains. These are also the values which are tested for convergence at the conclusion of each iteration.

2. *PBJ-ITMM-SI* Fourier Analysis

To theoretically analyze the iterative performance of *PBJ-ITMM-SI*, we employ a Fourier analysis. For this analysis, we consider an infinite homogeneous medium. We then use this problem to determine the scaling of the error from the combined iterative sequence. For simplicity, in the theoretical analysis we determine the scaling of the error in the cell averaged scalar flux due to *SI* followed by *PBJ-ITMM*. We verify computationally that this scaling is the same as the scaling of the error in the outgoing angular fluxes from *PBJ-ITMM* followed by *SI*, which is the practical order of execution for the method. By executing the theoretical analysis with *SI* followed by *PBJ-ITMM* though, we eliminate the angular shape of the error, thereby making the results cleaner.

To perform this Fourier analysis, we begin by subtracting Eqs. (4) from their converged form to obtain,

$$\nu_{x,m,k,j}\left(\delta\psi^{x+,(s+\frac{1}{2})}_{m,k,j} - \delta\psi^{x-,(s+\frac{1}{2})}_{m,k,j}\right) + \nu_{y,m,k,j}\left(\delta\psi^{y+,(s+\frac{1}{2})}_{m,k,j} - \delta\psi^{y-,(s+\frac{1}{2})}_{m,k,j}\right) + \delta\psi^{(s+\frac{1}{2})}_{m,k,j} = \frac{c_{k,j}}{4\pi}\delta\phi^{(s)}_{k,j} \quad (5a)$$

$$\delta\psi^{(s+\frac{1}{2})}_{m,k,j} = \frac{1+\alpha_{u,m,k,j}}{2}\delta\psi^{u+,(s+\frac{1}{2})}_{m,k,j} + \frac{1-\alpha_{u,m,k,j}}{2}\delta\psi^{u-,(s+\frac{1}{2})}_{m,k,j} \quad (5b)$$

$$\delta\phi^{(s+\frac{1}{2})}_{k,j} = \sum_{m=1}^{M} w_m \delta\psi^{(s+\frac{1}{2})}_{m,k,j} \quad (5c)$$

where,

$$\delta\psi^{(s)} \equiv \psi^{(\infty)} - \psi^{(s)} \quad (6)$$

Note that the iteration indexes in these equations are $\frac{1}{2}$ lower that in normal *SI* equations to reflect that *SI* is being performed first in the Fourier analysis. We now introduce the following Fourier *ansatz*.

$$\delta\phi^{(s)}_{k,j} = \Phi^{(s)}(\lambda_x,\lambda_y)\exp\left(i\Sigma_t(\lambda_x(k-\frac{1}{2})\Delta x + \lambda_y(j-\frac{1}{2})\Delta y)\right) \quad (7a)$$

$$\delta\psi^{(s+\frac{1}{2})}_{m,k,j} = f_m\Phi^{(s+\frac{1}{2})}(\lambda_x,\lambda_y)\exp\left(i\Sigma_t(\lambda_x(k-\frac{1}{2})\Delta x + \lambda_y(j-\frac{1}{2})\Delta y)\right) \quad (7b)$$

$$\delta\psi^{u\pm,(s+\frac{1}{2})}_{m,k,j} = \Phi^{(s+\frac{1}{2})}(\lambda_x,\lambda_y)g^u_m \times \exp\left(i\Sigma_t\left(\lambda_x(k-\frac{1}{2})\Delta x + \lambda_y(j-\frac{1}{2})\Delta y \pm \frac{\lambda_u sg(\Omega_{u,m})\Delta u}{2}\right)\right) \quad (7c)$$

In these equations, $\Phi(\lambda_x,\lambda_y)$ represents the magnitude of the iterative error in the scalar flux at the specified frequencies, f_m represents the angular shape of the iterative error in the cell averaged angular flux, and g^u_m represents the angular shape of the cell edge angular flux on the u face of the cell. Additionally, sg is the *signum* function.

We now substitute this Fourier *ansatz* into the residual auxiliary equation, Eq. (5b), solve for f_m, employ Euler's formula, and simplify to obtain the following expression.

$$f_m = g_m^u \Bigg[\cos\Big(\frac{\Sigma_t \lambda_u sg(\Omega_{u,m})\Delta u}{2}\Big) + \alpha_{u,m} i \sin\Big(\frac{\Sigma_t \lambda_u sg(\Omega_{u,m})\Delta u}{2}\Big)\Bigg] \quad (8)$$

We now substitute the *ansatz* into the residual balance equation, Eq. (5a). As we do this, we use the identity for f_m we just obtained as well as Euler's formula to obtain the following equation after simplifying.

$$\begin{aligned} &\nu_{u,m}\Phi^{(s+\frac{1}{2})}(\lambda_x,\lambda_y) g_m^u \Big(2i \sin\Big(\frac{\lambda_u sg(\Omega_{u,m})\Delta u}{2}\Big)\Big) \\ &+ \nu_{v,m}\Phi^{(s+\frac{1}{2})}(\lambda_x,\lambda_y) g_m^v \Big(2i \sin\Big(\frac{\lambda_v sg(\Omega_{v,m})\Delta v}{2}\Big)\Big) \\ &+ \Phi^{(s+\frac{1}{2})}(\lambda_x,\lambda_y) g_m^u \Bigg[\cos\Big(\frac{\Sigma_t \lambda_u sg(\Omega_{u,m})\Delta u}{2}\Big) \\ &+ \alpha_{u,m} i \sin\Big(\frac{\Sigma_t \lambda_u sg(\Omega_{u,m})\Delta u}{2}\Big)\Bigg] \\ &= \frac{c}{4\pi}\Phi^{(s)}(\lambda_x,\lambda_y) \end{aligned} \quad (9)$$

Note that in this equation we use the general indexes $u = x, y$ and $v = y, x$. We do this so that we obtain a general expression for g_m^u as opposed to separate expressions for g_m^x and g_m^y.

In order to eliminate the g_m^v term from this equation, we take into account that the left hand side of the residual auxiliary equation, Eq. (5b) does not depend on the choice of u. Therefore, we equate the right hand side of this equation with superscript u to the right hand side with superscript v. We then substitute the *ansatz*, Eq. (7c), and solve for g_m^v to obtain the following expression.

$$g_m^v = \beta_m^{u,v} g_m^u \quad (10)$$

where,

$$\beta_m^{u,v} \equiv \frac{\cos\Big(\frac{1}{2}\Sigma_t \lambda_u sg(\Omega_{u,m})\Delta u\Big) + \alpha_{u,m} i \sin\Big(\frac{1}{2}\Sigma_t \lambda_u sg(\Omega_{u,m})\Delta u\Big)}{\cos\Big(\frac{1}{2}\Sigma_t \lambda_v sg(\Omega_{v,m})\Delta v\Big) + \alpha_{v,m} i \sin\Big(\frac{1}{2}\Sigma_t \lambda_v sg(\Omega_{v,m})\Delta v\Big)} \quad (11)$$

We now substitute Eq. (10) into Eq. (9) to eliminate g_m^v. With this term eliminated, we can now solve the resulting equation to obtain the following expression to represent the iterative error in the outgoing angular fluxes.

$$\begin{aligned} &\Phi^{(s+\frac{1}{2})}(\lambda_x,\lambda_y) g_m^u \\ &= \frac{\frac{c}{4\pi}\Phi^{(s)}(\lambda_x,\lambda_y)}{\Bigg[2i\nu_{u,m}\sin\Big(\frac{1}{2}\lambda_u sg(\Omega_{u,m})\Delta u\Big) + 2i\nu_{v,m}\beta_m^{u,v}\sin\Big(\frac{1}{2}\lambda_v sg(\Omega_{v,m})\Delta v\Big) \\ &+ \cos\Big(\frac{1}{2}\Sigma_t \lambda_u sg(\Omega_{u,m})\Delta u\Big) + \alpha_{u,m} i \sin\Big(\frac{1}{2}\Sigma_t \lambda_u sg(\Omega_{u,m})\Delta u\Big)\Bigg]} \end{aligned} \quad (12)$$

With an expression for the scaling of the iterative error due to the *SI* step, we now examine the *PBJ-ITMM* step. *PBJ-ITMM* with *AHOT-N0* has been examined previously by Fourier analysis.[5] During this analysis, the following expression is obtained for the mapping of the error in the incoming angular flux to the resulting error in the cell averaged scalar flux after the *PBJ-ITMM* iteration. Since scalar flux is what *PBJ-ITMM* passes to *SI* and we are not interested in the angular shape of the error, we begin with this expression to determine the mapping of the error in the scalar flux before the *SI* step to the error in the scalar flux after the two step iterative process. The derivation of the following expression is available in [5].

$$\delta\phi_{k,j}^{(s+1)} = \sum_{m=1}^{M}\Big(\gamma_{m,k,j}^x \delta\psi_{m,k,j}^{x-,(s+\frac{1}{2})} + \gamma_{m,k,j}^y \delta\psi_{m,k,j}^{y-,(s+\frac{1}{2})}\Big) \quad (13)$$

where,

$$\gamma_{m,k,j}^u \equiv w_m \eta_{k,j} \frac{\zeta_{u,m,k,j}}{1+\zeta_{x,m,k,j}+\zeta_{y,m,k,j}} \quad (14a)$$

$$\eta_{k,j} \equiv \left(1 - \frac{c_{k,j}}{4\pi}\sum_{m=1}^{M} w_m \frac{1}{1+\zeta_{x,m,k,j}+\zeta_{y,m,k,j}}\right)^{-1} \quad (14b)$$

and

$$\zeta_{u,m,k,j} = \frac{2\nu_{u,m,k,j}}{1+\alpha_{u,m,k,j}} \quad (14c)$$

We now introduce the following *ansatz* for the *PBJ-ITMM* step.

$$\delta\phi_{k,j}^{(s+1)} = \Phi^{(s+1)}(\lambda_x,\lambda_y)\exp\Big(i\Sigma_t(\lambda_x(k-\frac{1}{2})\Delta x + \lambda_y(j-\frac{1}{2})\Delta y)\Big) \quad (15a)$$

$$\begin{aligned} &\delta\psi_{m,k,j}^{u\pm,(s+\frac{1}{2})} = \Phi^{(s+\frac{1}{2})}(\lambda_x,\lambda_y) g_m^u \\ &\times \exp\Big(i\Sigma_t\Big(\lambda_x(k-\frac{1}{2})\Delta x + \lambda_y(j-\frac{1}{2})\Delta y \pm \frac{\lambda_u sg(\Omega_{u,m})\Delta u}{2}\Big)\Big) \end{aligned} \quad (15b)$$

We substitute these two expressions into Eq. (13) and simplify to obtain,

$$\Phi^{(s+1)}(\lambda_x,\lambda_y) = \sum_{m=1}^{M}\left[\gamma_m^x \Phi^{(s+\frac{1}{2})}(\lambda_x,\lambda_y) g_m^x \exp\left(\frac{-i\Sigma_t\lambda_x sg(\Omega_{x,m})\Delta x}{2}\right) + \gamma_m^y \Phi^{(s+\frac{1}{2})}(\lambda_x,\lambda_y) g_m^y \exp\left(\frac{-i\Sigma_t\lambda_y sg(\Omega_{x,y})\Delta y}{2}\right)\right] \quad (16)$$

Recall that from the *SI* step we obtained an expression for $\Phi^{(s+\frac{1}{2})}(\lambda_x,\lambda_y)g_m^u$, Eq. (12). Therefore, to obtain the scaling of the error in the scalar flux after the combined iterative sequence, we substitute this expression into the previous equation and divide by $\Phi^{(s)}(\lambda_x,\lambda_y)$ to obtain,

$$\frac{\Phi^{(s+1)}(\lambda_x,\lambda_y)}{\Phi^{(s)}(\lambda_x,\lambda_y)} = \sum_{m=1}^{M}\left[\gamma_m^x \chi_m^{x,y} \exp\left(\frac{-i\Sigma_t\lambda_x sg(\Omega_{x,m})\Delta x}{2}\right) + \gamma_m^y \chi_m^{y,x} \exp\left(\frac{-i\Sigma_t\lambda_y sg(\Omega_{y,m})\Delta y}{2}\right)\right] \quad (17)$$

where we define,

$$\chi_m^{u,v} \equiv \frac{\frac{c}{4\pi}}{\left[2i\nu_{u,m}\sin\left(\frac{1}{2}\lambda_u sg(\Omega_{u,m})\Delta u\right) + 2i\nu_{v,m}\beta_m^{u,v}\sin\left(\frac{1}{2}\lambda_v sg(\Omega_{v,m})\Delta v\right) + \cos\left(\frac{1}{2}\Sigma_t\lambda_u sg(\Omega_{u,m})\Delta u\right) + \alpha_{u,j} i \sin\left(\frac{1}{2}\Sigma_t\lambda_u sg(\Omega_{u,m})\Delta u\right)\right]} \quad (18)$$

Equation (17) is the final result of the Fourier analysis of *PBJ-ITMM-SI*, providing the scaling of the error in the cell average scalar flux as a function of the two Fourier variables for the combined iterative sequence. We will also refer to this expression as the eigenvalues, as the scaling of the combined iterative sequence represents the eigenvalues of the iterative operator.

III. RESULTS AND ANALYSIS

We compliment our theoretical analysis with a series of computational experiments. First, we verify the *PBJ-ITMM* capabilities of our FORTRAN code by comparing the spectral radius estimates produced to those previously presented for *PBJ-ITMM* with *AHOT-N0*. We then use this code to computationally verify the Fourier analysis for *PBJ-ITMM-SI*. With the analysis verified, we provide additional computational experiments including a study of *PBJ-ITMM-SI*'s performance in heterogeneous mediums. We aim the analysis at exploring the strengths and weaknesses of *PBJ-ITMM-SI*, as well as demonstrate where the results give insight which expands our overall understanding of *PBJ-ITMM*.

1. PBJ-ITMM Code Verification

Before presenting the results for *PBJ-ITMM-SI*, we briefly verify the *PBJ-ITMM* capabilities of our code, as well as provide visual aid for the previously discussed iterative slowdown in optically thin cells. We display the computationally estimated spectral radii for *PBJ-ITMM* in Fig. 1. For this simulation, we use a one cell problem with all reflective boundary conditions to model the infinite homogeneous medium of the Fourier analysis. Note that all computational spectral radius esimates in this paper are obtained as the ratio of the L_2 norms of the iterative change in the outgoing angular fluxes for two successive iterations.

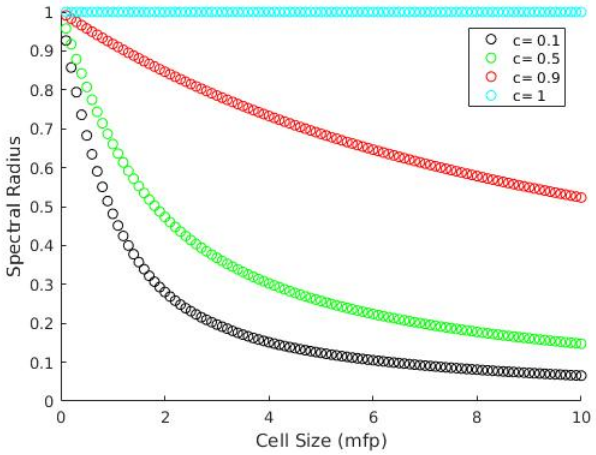

Fig. 1. Numerically estimated spectral radius of *PBJ-ITMM* for one cell with all reflective boundary conditions.

These computationally estimated spectral radii show agreement with the previously obtained results shown in the literature.[5]

2. PBJ-ITMM-SI Fourier Analysis Results

With the *PBJ-ITMM* capabilities of our code verified as well as a frame of reference provided for comparison, we examine the performance of *PBJ-ITMM-SI*. The theoretical results were obtained using *Mathematica*. We begin by plotting the real component of Eq. (17), the eigenvalues which govern the iterative performance of *PBJ-ITMM-SI* versus λ_y for various values of λ_x, Figs. 2 - 5.

From these eigenvalues, we are able to conclude that the flat mode ($\lambda_x = \lambda_y = 0$) is the slowest converging mode for *PBJ-ITMM-SI*. This is easily seen as the eigenvalues are maximized for any given λ_x at $\lambda_y = 0$ Additionally, if we were to chose any λ_y value and compare the eigenvalues between the four graphs, we see that the graph for $\lambda_x = 0$ clearly has the largest magnitude eigenvalue for all cases. One final note is that we only display the real component of the eigenvalues despite Eq. (17) having an imaginary component. We expect the eigenvalues for *PBJ-ITMM-SI* to be only real and that the imaginary components all cancel out. This was confirmed by plotting each of these graph for the imaginary component, verifying that they were all zero.

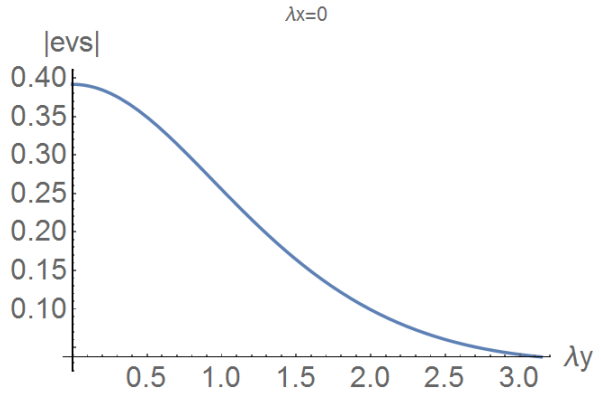

Fig. 2. Theoretical *PBJ-ITMM-SI* eigenvalues for $\lambda_x = 0$.

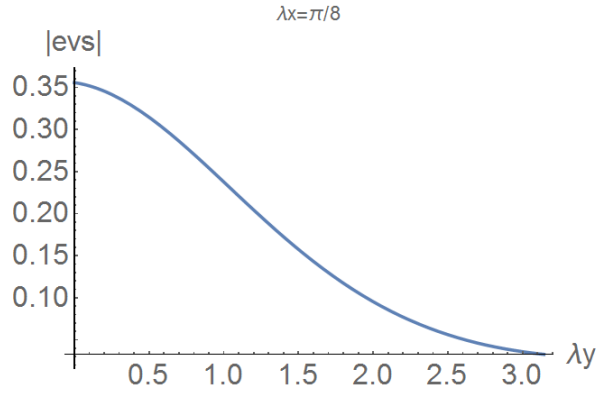

Fig. 3. Theoretical *PBJ-ITMM-SI* eigenvalues for $\lambda_x = \frac{\pi}{8}$.

Confirming that the flat mode is in fact the dominant mode for *PBJ-ITMM-SI*, we plot this eigenvalue versus cell size to observe the effect of *SI* preconditioning. In this graph, Fig. 6, the lines represent the theoretical predictions generated using *Mathematica* and the points represent the computational estimates. These computational estimates were obtained using a single cell, all reflective boundary condition problem to simulate the conditions of the Fourier analysis.

Before analyzing these results, it is important to note two facts about the method in which these computational estimates were obtained. Firstly, recall that the Fourier analysis was performed to obtain the scaling of the error in the cell averaged scalar flux due to an *SI* iteration followed by a *PBJ* iteration. In application, the iterative steps are the reverse of this, and the convergence of *PBJ-ITMM* is formally based on the subdomain interface angular fluxes. To confirm that our Fourier analysis is valid for the practical implication of *PBJ-ITMM-SI*, the computational estimates were obtained by executing *PBJ-ITMM* followed by *SI*, then estimating the spectral radius using the outgoing angular fluxes.

Additionally, the *SI* operator only lags the scalar flux in the scattering source. In practice however, the incoming angular flux at the boundaries must also be lagged in the case of reflective boundary conditions. This eliminates the synchronous behavior of *SI* desired and in the case of our single cell test problem, actually makes *SI* equivalent to *Inexact Parallel Block Jacobi* (*IPBJ*).[7] As we will present later, this has a negative impact on the iterative performance. To avoid this and represent the *SI* step as dictated by Eqs. (4), we modify the *SI* routine in our code to converge the incoming angular fluxes to balance with the lagged scattering source before proceeding to the *PBJ-ITMM* step.

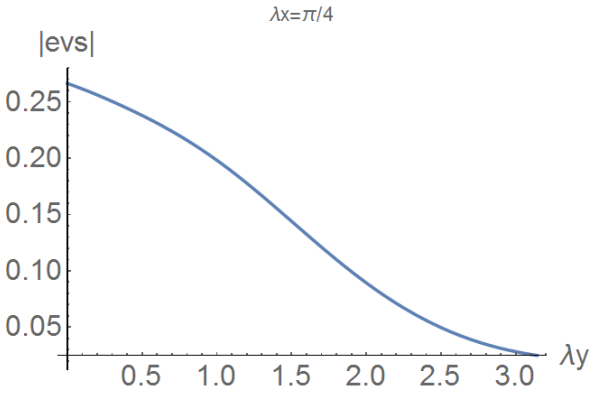

Fig. 4. Theoretical *PBJ-ITMM-SI* eigenvalues for $\lambda_x = \frac{\pi}{4}$.

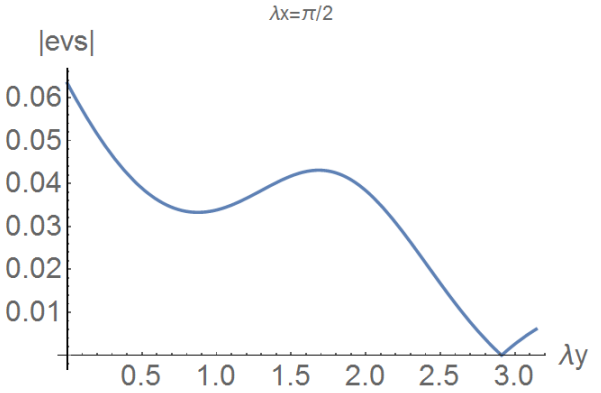

Fig. 5. Theoretical *PBJ-ITMM-SI* eigenvalues for $\lambda_x = \frac{\pi}{2}$.

Upon analyzing Fig. 6, the first thing we note is that the computational results confirm the theoretical predictions. We also see that for all c values less than one, the spectral radius no longer approaches unity as cell size decreases. Without *SI* preconditioning, as the cell size is decreased, cells become

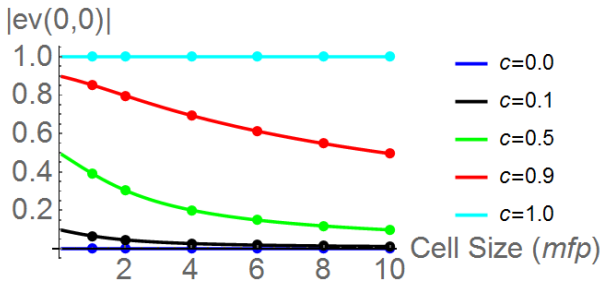

Fig. 6. Theoretically predicted (lines) and numerically estimated (points) flat mode eigenvalues of *PBJ-ITMM-SI*.

more mathematically coupled to distant cells (i.e. two distant cells' solutions become more dependent on each other). Since *PBJ-ITMM* exchanges information between sub-domains only in between iterations, this significant coupling between cells that become separated by a number of cells which grows unbounded as the cell size decreases indicates that the number of iterations required for these two cells to become "aware" of a change to the others' solution also grows without bound, resulting in a lack of robustness. We see that *SI* preconditioning achieved the desired iterative properties. While the spectral radius is still larger in optically thin cells than in uniformly thicker cells, the spectral radius remains bounded below unity for all scattering ratios < 1, thereby achieving the desired robustness. As stated previously, we conjecture that this is due to *SI*'s synchronous nature which allows all cells to become "aware" of a change to another cell's solution, on which its own solution is dependent.

A feature of the *PBJ-ITMM-SI* spectrum which must be noted is that *SI* preconditioning is far more effective at reducing the spectral radius for low scattering ratios. This is to be expected as the lagged scalar flux in the scattering source of the *SI* equations is known to cause ineffectiveness in problems with scattering ratios close to unity. This unfortunately leads to the smallest amount of benefit from *SI* preconditioning in the slowest converging problems. Returning to the physical interpretation of the *PBJ-ITMM-SI* iterative process, *PBJ-ITMM* resolves particle collisions locally within a sub-domain, and the *SI* step then allows these particles to stream through the medium until their next collision. In a problem with a high scattering ratio and optically thin cells though, particles can scatter and consequently travel far across the domain many times. The inability of *SI* to resolve collisions over the course of a single iteration renders it ineffective at accounting for this effect. For this reason, the ideal acceleration method for *PBJ-ITMM* would be one which allows for information to be transmitted synchronously across the entire spatial domain and also for the resolution of collisions. Despite this shortcoming though, *SI* preconditioning achieves iterative robustness for all problems where $c < 1$, preventing the number of required iterations from increasing without bound as cell size decreases.

Recall that the computational test problem used to verify the Fourier analysis used one cell with all reflective boundary conditions. A problem with one cell only excites the flat error mode. Although observation of the individual modes shows the flat mode to be the limiting mode, we conduct a finite medium test to ensure that this is the case. From Table I, we see that as the number of cells increases, the spectral radius approaches the value estimated for the infinite medium by the one cell test problem with reflective boundary conditions. This confirms that the flat mode is the dominant mode, and hence, governs convergence rate.

3. PBJ-ITMM-SI with Reflective or Periodic Boundary Conditions

We must make note of an effect observed when these spectral radius estimates were obtained with lagged boundary incoming angular fluxes, as would be the case in actual implementation of a code to a problem with periodic or reflective boundary conditions. When we estimate the spectral radius of *PBJ-ITMM-SI* with lagged boundary conditions, we obtain the spectral radius estimates shown in Fig. 7 for the infinite homogeneous medium.

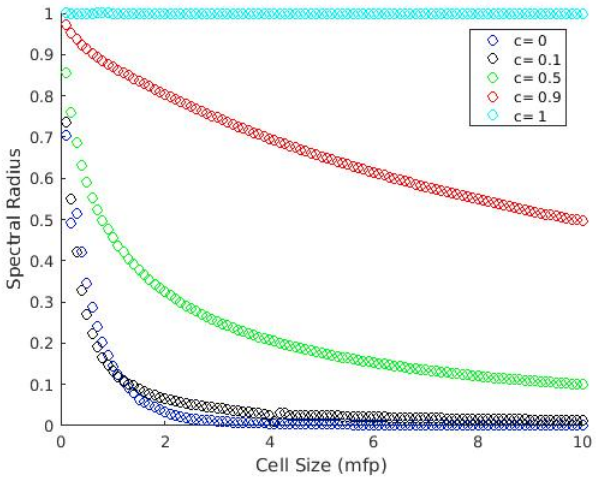

Fig. 7. Computational spectral radius estimations for *PBJ-ITMM-SI* with lagged boundary conditions.

As expected, when the boundary conditions are lagged, we lose robustness in optically thin cells. This is due to the fact that the *SI* step is no longer completely synchronous. If we consider a quadrant-symmetric nuclear reactor core which is modeled by a quarter core with two reflective boundary conditions, these reflective boundary conditions are lagged by an iteration, effectively decoupling the four quadrants of the reactor core over the course of an iteration, allowing them to exchange information once between two consecutive iterations. This generates the same mathematical decoupling of cells which are physically coupled in *SI* that we are implementing *SI* preconditioning to alleviate. This phenomenon renders *SI* preconditioning ineffective for problems with reflective or periodic boundary conditions.

From this behavior, we make note of another important quality which a method must have in order to effectively accelerate *PBJ-ITMM*. If the solution method is to be applicable to problems with reflective or periodic boundary conditions, then the acceleration method must be one which does not lag these boundary conditions. We see from Fig. 7 that the lagging of this boundary condition eliminates the synchronous nature and consequently, the robustness in optically thin cells.

While this does impose a restriction on the methods which can be used to effectively accelerate *PBJ-ITMM*, it also supports our theory of the underlying cause of its iterative slowdown. We attribute the slowdown in optically thin cells to *PBJ-ITMM*'s asynchronous nature, and the reduction of this slowdown in *PBJ-ITMM-SI* to the synchronous nature of *SI*. These results further support this theory, as the removal of *SI*'s synchronous nature caused it to be ineffective at speeding up *PBJ-ITMM* in optically thin cells, suggesting that the speedup observed when the boundary conditions were not lagged was chiefly due to the synchronicity of *SI*.

	$c = 0.1$			$c = 0.5$			$c = 0.9$		
	$0.5mfp$	$1mfp$	$5mfp$	$0.5mfp$	$1mfp$	$5mfp$	$0.5mfp$	$1mfp$	$5mfp$
$N = 2$	0.0191	0.0233	0.0107	0.1043	0.1369	0.0814	0.2059	0.2980	0.3086
$N = 4$	0.0424	0.0451	0.0179	0.2294	0.2639	0.1362	0.4518	0.5734	0.5158
$N = 8$	0.0623	0.0585	0.0210	0.3386	0.3424	0.1601	0.6677	0.7448	0.6074
$N = 16$	0.0744	0.0639	0.0219	0.4046	0.3760	0.1677	0.7985	0.8187	0.6380
$N = 32$	0.0792	0.0657	0.0222	0.4321	0.3867	0.1699	0.8534	0.8431	0.6466
$N = 64$	0.0807	0.0663	0.0224	0.4406	0.3897	0.1708	0.8713	0.8500	0.6490
$N = 128$	0.0812	0.0667	0.0224	0.4431	0.3908	0.1711	0.8762	0.8518	0.6500
∞	0.0813	0.0661	0.0201	0.4453	0.3913	0.1715	0.8781	0.8531	0.6505

TABLE I. Spectral Radius Estimates for Finite Medium Approaching That of Infinite Medium as Number of Cells Increases. (∞ corresponds to the spectral radius estimate of the infinite medium).

4. Comparison of SI, PBJ-ITMM, and PBJ-ITMM-SI

Since *PBJ-ITMM-SI* is the combination of two iterative transport solution methods, we compare the combined iterative method to each of the individual methods to determine the added benefit of combining them in different problems. We begin with the spectral radius trends for *PBJ-ITMM-SI* in Fig. 6. We see that for the combined iterative method, the spectral radius approaches the scattering ratio as the cell size decreases. We also know the spectral radius of *SI* to be the scattering ratio.[8] This indicates that as the cell size decreases, the *PBJ-ITMM* iterations begin to have no effect on the rate of convergence. To explain this phenomenon, we refer to our physical interpretations of the iterations, that the *PBJ-ITMM* iteration simulates particles scattering within a sub-domain until they leave, and an *SI* iteration simulates particles streaming across the medium until they collide. With this in mind, for particles which stream uncollided through a sub-domain, the *PBJ-ITMM* produces no additional information, as the *SI* iteration would have accounted for this uncollided streaming anyway. Therefore, as the cell size decreases and the fraction of particles which travel uncollided through a sub-domain tends towards 1, the *PBJ-ITMM* iteration contributes nothing to the combined iterative process and the convergence becomes based solely on *SI*. Analogously, we can predict the opposite to be true as well; as the cell size increases, the spectral radius of *PBJ-ITMM-SI* should approach that of *PBJ-ITMM*. To defend this claim, we return to our physical interpretation of the iterative sequence. Based on this interpretation, *SI* contributes nothing to the simulation of particles which enter the sub-domain and collide before exiting, as this event would be simulated by the *PBJ-ITMM* iteration. Therefore, as the cell size increases and the fraction of particles entering a sub-domain which then interact within that sub-domain approaches 1, the *SI* iteration contributes nothing to the combined sequence, causing the *PBJ-ITMM-SI* spectral radius to tend towards that of *PBJ-ITMM*. We demonstrate this behavior using the spectral radius of an infinite medium in Fig. 8 and the iteration counts required to converge a finite medium problem to a stopping criterion of 10^{-12} in Table II. (Note that the *SI* spectral radius is omitted from the graph as we know it to be the scattering ratio).

From this graph and table we observe the trend just described, where the convergence rate *PBJ-ITMM-SI* approaches that of *SI* in optically thin cells and that of *PBJ-ITMM* in optically thick cells. We therefore see that when cells are optically thin enough or thick enough, the addition of an extra step in the iteration becomes irrelevant to the convergence rate. The appropriate single step iterative method would be more effective in these cases. However, we see from the graph and table that there exists a range of cell sizes, specific to each scattering ratio, over which *PBJ-ITMM-SI* yields a significant reduction in spectral radius and required iterations over both of the individual methods.

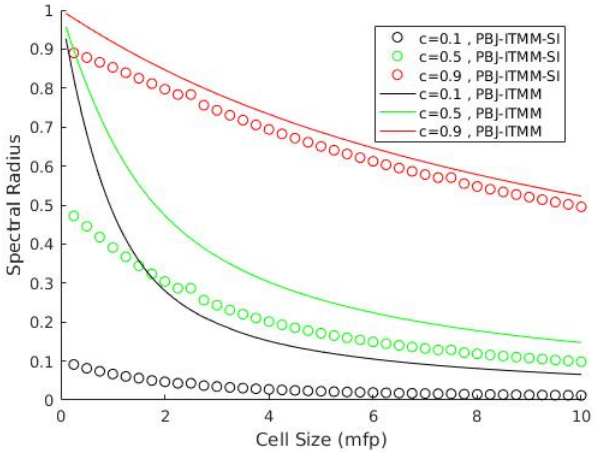

Fig. 8. Spectral radius for *PBJ-ITMM* and *PBJ-ITMM-SI*.

This provides our final insight into guidelines for developing future acceleration methods for *PBJ-ITMM*. As we have discussed, the favorability of *SI* over *PBJ-ITMM-SI* in very thin cells comes from the fact that the way in which *SI* preconditioning alleviates *PBJ-ITMM*'s lack of robustness ultimately begins to include all of the effects captured by *PBJ-ITMM* as the cells become optically thin. Therefore, for a future acceleration method, it would be beneficial to investigate a method involving a low-order operator which involves approximations in order to allow streaming between cells and multiple scattering interactions to be modeled in a single iteration. This would allow for *PBJ-ITMM* to still have an effect in approach to convergence by resolving local imperfections in the approx-

		$0.5mfp$	$1mfp$	$5mfp$	$10mfp$
	SI	15	15	14	14
$c = 0.1$	*PBJ-ITMM*	96	49	15	12
	PBJ-ITMM-SI	14	13	9	8
	SI	46	45	42	41
$c = 0.5$	*PBJ-ITMM*	140	73	23	16
	PBJ-ITMM-SI	40	34	18	14
	SI	289	286	270	264
$c = 0.9$	*PBJ-ITMM*	687	350	80	47
	PBJ-ITMM-SI	238	193	70	43

TABLE II. Iterations required for 100x100 problems of various composition for *SI*, *PBJ-ITMM*, and *PBJ-ITMM-SI*. $c = 1$ is neglected from this table as it was not seen to converge in 1000 iteration for any of these cases. Stopping Criterion: 10^{-12}

imate solution, while also potentially reducing the slowdown due to increased scattering ratio.

5. PBJ-ITMM-SI in Heterogeneous Problems

Given the previous comparison of *PBJ-ITMM-SI* to its individual iterative methods, we appear to have somewhat of a problem. We proposed *SI* preconditioning in order to make *PBJ-ITMM* robust in optically thin cells, which it did; but as we saw, in optically thin cells, unaccelerated *SI* is actually a better option. This analysis was only conducted on homogeneous test problems though. Almost any real-world problem will be heterogeneous, where *PBJ-ITMM-SI* has the potential to be an effective iterative method. If a problem contains both optically thin and thick cells, then our physical interpretation of the iterations tells us that the *PBJ-ITMM* iterations will allow the numerous local collisions in the optically thick cells to be resolved saving many *SI* iterations, and particles can be simulated streaming across the optically thin cells in a single *SI* iteration, saving the many *PBJ-ITMM* iterations required for this to be modeled.

To test this theory, we develop a problem with optically thick cells adjacent to optically thin cells. The geometry of this problem is shown in Fig. 9. A 100x100 cell mesh is imposed on this problem, making each stripe 10 cells wide. Each cell within the "thick" regions is 10 *mfp* thick and each cell within the "thin" region is 0.1 *mfp* thick. All boundary conditions are vacuum. We observe the required number of iterations to converge this problem using *SI*, *PBJ-ITMM*, and *PBJ-ITMM-SI* for various scattering ratios. The iterations required to converge the solution to a stopping criterion of 10^{-12} are tabulated in Table III.

From the iteration table, we confirm that *PBJ-ITMM-SI* shows a significant improvement over each of the individual methods. As we have discussed, we attribute this to the fact that the two iterative methods do not rely on one another to resolve parts of a problem which the other is ineffective at. Each method simply resolves the parts of the simulation which it is more effective at with little to no aid from the other method. We can see from the required number of *PBJ-ITMM* iterations that optically thin cells within a problem cause significant iterative slowdown even if the entire domain

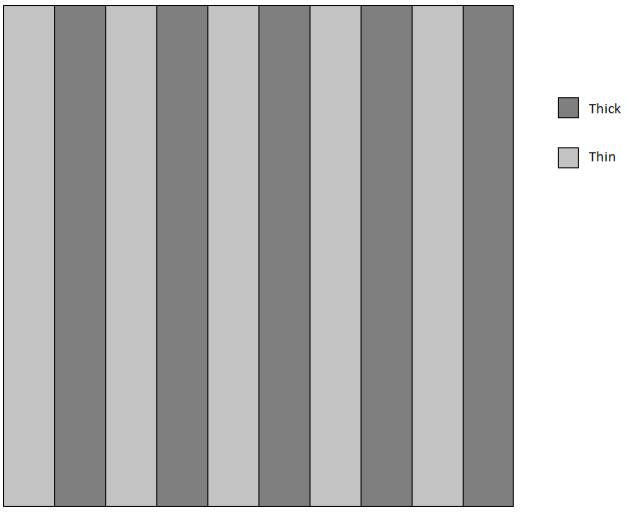

Fig. 9. Geometry of the heterogeneous stripe problem. "Thick" regions contain cells which are 10 *mfp* thick and "thin" regions contain cells which are 0.1 *mfp* thick. A 100x100 cell mesh is used making each stripe 10 cells wide. All boundary conditions are vacuum.

is not optically thin. *SI* preconditioning is seen to dramatically reduce this slowdown by allowing *SI* to simulate the streaming of particles through the optically thin regions and *PBJ-ITMM* to simulate the local scattering of particles within the optically thick regions.

Since most realistic problem will contain cells of a variety of optical thicknesses, we conclude that *SI* preconditioning is an effective method for alleviating the iterative slowdown *PBJ-ITMM* experiences due to optically thin cells. In homogeneous problems, we saw that there was a relatively small range of cell sizes over which *PBJ-ITMM-SI* showed a significant improvement on both of the individual methods for $c > 0.5$. With a realistic heterogeneous problem containing cells from the two regions of cell sizes where each of the two individual iterative methods are most favorable though, we see that each part of the two step method is able to resolve the portion of the simulation for which it is intended, resulting in a significant

c	*SI*	*PBJ-ITMM*	*PBJ-ITMM-SI*
0.1	14	113	12
0.2	20	132	16
0.3	26	150	19
0.4	33	169	22
0.5	43	191	26
0.6	58	217	31
0.7	82	252	37
0.8	130	305	46
0.9	272	414	67
1.0	N/C	N/C	N/C

TABLE III. Required number of *SI*, *PBJ-ITMM*, *PBJ-ITMM-SI* iterations for convergence of the heterogeneous stripe problem depicted in Fig. 9. N/C indicates lack of convergence in 1000 iterations. Stopping Criterion: 10^{-12}

improvement over each individual method. We also note that the largest improvement due to *SI* preconditioning was seen to occur in problems with larger scattering ratios (other than $c = 1$). This is an excellent result, as it indicates that for realistic problems, *SI* preconditioning provides the largest amount of acceleration in problems which are the slowest converging.

IV. CONCLUSIONS

We have studied the effects of *SI* preconditioning on the iterative properties of *PBJ-ITMM* through theoretical analysis and a variety of computational experiments. Through this analysis we have determined *SI* preconditioning to be effective at reducing *PBJ-ITMM*'s iterative slowdown in problems with optically thin cells due to *SI*'s synchronous nature. Through our studies of homogeneous problems, we determined that each method of the two step process was more effective than the other at simulating cells of certain optical thicknesses, and that this resulted in the other method contributing little or nothing to the iterative convergence of these cells. However, when we expanded our study to observe the effect of *SI* preconditioning in heterogeneous problems which contain cells of varying optical thickness, we observed that the methods executed in sequence were able to converge the problems with higher scattering ratios in far fewer iterations than either of the methods could independently, rendering *SI* preconditioning an effective acceleration method for *PBJ-ITMM* in realistic problems.

We must mention once more though, that this reduction in required iterations comes at the cost of only half of the iterative sequence being solved on a massively parallel system, due to the complex sweep algorithms which *SI* requires to be executed in parallel on unstructured grids being the very feature *PBJ-ITMM* was invented to avoid. We see though, that although *PBJ-ITMM-SI* does not provide a fully parallel method, it allows for half of the iterative sequence to be executed in a massively parallel fashion, while avoiding the unbounded increase in required iterations as cells become optically thin that is associated with *PBJ-ITMM*. Additionally, each direction's mesh sweep in *SI* can be conducted simultaneously, making it parallel.

Finally, we note challenges that still remain. Most obviously, development of an acceleration method which has a less steep penalty to the level of parallelization would be ideal and we have provided comments throughout our study which could aid in the development of such a method. Through our study of *SI* preconditioning, we have determined that the mathematical decoupling of distant sub-domains over the course of an iteration is the cause of *PBJ-ITMM*'s iterative slowdown in optically thin cells, as this becomes increasingly inaccurate as these sub-domains become more physically coupled. While *SI* preconditioning eliminates this behavior, it does not allow for resolution of scattering collisions. We have made note that an acceleration method which attempts to approximate the full transport solution, simulating both the long-distance streaming of particles as well as the resolution of collisions, would be a valuable study. Such a method would then rely on *PBJ-ITMM* to resolve the local inaccuracies of the acceleration method's solution. Lastly, we note that although *SI* preconditioning greatly improved the iterative effectiveness of *PBJ-ITMM* in realistic problems, it still remains ineffective in problems with a scattering ratio of 1. Resolving this issue remains as a future challenge.

V. ACKNOWLEDGMENTS

This material is based upon work by the two authors (DSH and YYA) supported by the Department of Energy National Nuclear Security Administration under Award Number(s) DE-NA0002576.

REFERENCES

1. R. J. ZERR and Y. Y. AZMY, "Solution of the Within-Group Multidimensional Discrete Ordinates Transport Equations on Massively Parallel Architectures, invited, Mark Mills Award Winner," *Transactions of the American Nuclear Society*, **105**, 229 (2011).
2. D. ANISTRATOV and Y. AZMY, Y., "Iterative Properties of the Integral Transport Matrix Method for the DD Scheme in 2D Cartesian Geometry," *PHYSOR 2014 - The role of Reactor Physica toward a Sustainable Future* (2014).
3. C. BAKER, "High Performance Radiation Transport Simulations: Preparing for Titan," *In Proceedings of the In-*

ternational Conference on High Performance Computing, Networking, Storage and Analysis (SC 12). (2012).

4. S. PLIMPTON, "Parallel Algorithms for Radiation Transport on Unstructured Grids," *SC '00: Proceedings of the 2000 ACM/IEEE Conference on Supercomputing*.
5. Y. Y. AZMY, D. ANISTRATOV, and R. J. ZERR, "Numberical and Analytical Studies of the Spectrum of Parallel Block Jacobi Iterations for Solving the Weighted Diamond Difference Form of the S_N Equations," *Joint International Conference on Mathematics and Computation (M&C), Supercomputing in Nuclear Applications (SNA) and the Monte Carlo (MC) Method* (2015).
6. Y. AZMY, Y., "The weighted Diamond Difference Form of Nodal Transport Methods," *Nuclear Science and Engineering*, **98** (1988).
7. M. ROSA, J. S. WARSA, and J. H. CHANG, "Fourier Analysis of Inexact Parallel Block-Jacobi Splitting with Transport Synthetic Acceleration," *Nuclear Science and Engineering*, **164**, 248–263 (2009).
8. E. LARSEN, "Unconditionally Stable Diffusion-Synthetic Acceleration Methods for the Slab Geometry Discrete Ordinates Equations. Part 1 Theory," *Nuclear Science and Engineering*, **82**, 47–63 (1982).